

EVALUATION OF MATERIAL PROPERTIES AND DESIGN REQUIREMENTS FOR BIODEGRADABLE MAGNESIUM STENTS

Stefano Farè¹, Qiang Ge¹, Maurizio Vedani¹, Gianmarco Vimercati¹
Dario Gastaldi², Francesco Migliavacca², Lorenza Petrini²
Stefano Trasatti³

Summary

Magnesium represents a very attractive material for biodegradable stents since the process of its natural and gradual dissolution into the human body by a corrosion process would prevent restenosis risks and would allow the progressive transmission of the mechanical load to the surrounding tissues after several months of service.

The objective of the present work is to develop a frame of mechanical and microstructural data about several commercially available Mg alloys in view of their use for biodegradable stents. The AZ31, AZ61, AZ80, ZM21, ZK61 and WE43 alloys in the form of extruded bars were thus investigated to compare their mechanical properties and corrosion resistance. Further high-temperature characterization was carried out by compression tests at high temperature (temperature range: 260-450°C, strain rate range: $5 \cdot 10^{-4} \div 3 \cdot 10^{-2} \text{ s}^{-1}$) in order to assess the optimal processing window for stent precursors manufacturing (small tubes 1÷2 mm in diameter) by hot extrusion.

The experimental results made available by this investigation were adopted to support the development of a finite element (FE) framework combining a shape optimization procedure and a detailed model for Mg alloy mechanical and corrosion damage behavior.

Keywords: magnesium, stent design, mechanical properties

TMS-ABM International Materials Congress, 26-30/07/2010 Rio de Janeiro, Brazil
Symposium: Characterization and Application of Biomaterials

¹ Department of Mechanical Engineering, Politecnico di Milano

² Laboratory of Biological Structure Mechanics, Department of Structural Engineering, Politecnico di Milano

³ Department of Physical Chemistry and Electrochemistry, University of Milan

Introduction

Biodegradable stents are attracting the attention of many researchers in biomedical and materials research fields since they can absolve their specific function for the expected period of time and then gradually disappear. This feature allows avoiding the risk of long-term complications such as restenosis or mechanical instability of the device when the vessel grows in size in peadiatric patients [1]. Magnesium and its alloys are very promising for this application since they feature a relatively low corrosion resistance in human-body fluids, and a good biocompatibility of both the metal itself and the corrosion reaction products [2-5].

One of the critical issues to be improved for achieving higher performances of biodegradable magnesium stents is the control of the corrosion kinetics in order to widen the period of time when the scaffolding action of the stent is effectively exerted. At present, the life-time of magnesium stents is of the order of a few months in physiological fluid environments while the optimal temporary function is required for a period of the order of six months [6,7]. Strategies to overcome this drawback include changing the composition of the alloy and tailoring its microstructure to improve the intrinsic corrosion resistance, adopting surface modification and coatings to temporarily insulating the bulk metallic structure or changing the stent design [3,8].

Stent design based on Finite Element (FE) actually revealed to be a reliable approach for defining innovative web shapes with improved scaffolding ability, reduced strain during expansion and extended degradation times due to higher mesh width of the stent [9]. Continuum damage models were also implemented in FE analyses in order to evaluate the degradation due to uniform and localized corrosion effects, this latter being ruled by the stress field generated during stent expansion [10]. Among the factors of importance on stent performance, the processing route plays a paramount role since grain size of the alloy, second-phase distribution, mechanical properties as well as absence of structural defects strongly depends on it. Hot extrusion is one of the most common processes used for small tube manufacturing that represent the precursors used for stent mesh cutting by laser. However, issues related to hot workability properties of the material for such small devices are not fully understood and limited information has been found in recent literature on this subject [11-14]. In this study, the room-temperature tensile properties, corrosion behavior and hot formability properties of several magnesium alloys have been investigated in view of their possible use for biodegradable stent manufacturing. The data and information generated by this investigation will be of use in future studies for the laboratory scale manufacturing of small stent precursors.

Materials and experimental procedures

A set of commercially available wrought Mg alloys were investigated in this study. The AZ31, AZ61, AZ80, ZM21, ZK61 and WE43 alloys were considered in the form of extruded bars with a diameter of 15 mm. All the alloys were studied in the as extruded condition (without any additional thermal treatment) since previous investigations already showed that no significant improvement in ductility was achievable by a solution annealing treatment. Microstructural investigations were carried out on longitudinal and transversal sections of the bars by grinding and polishing the materials according to standard metallographic techniques. Etching for

optical and scanning electron microscopy was performed by using the Nital reagent (2% HNO₃ in ethylene).

Disk-shaped specimens 15 mm in diameter and 5 mm thick were used for long-term exposure corrosion tests. Mass loss measurements were carried out under atmospheric pressure in 250 ml jacketed glass cells, where specimens were immersed in synthetic body fluid (SBF) solutions with tris(hydroxymethyl) aminomethane added as buffering agent. Weight loss experiments were performed in duplicate for each alloy and lasted 90 hours. The surface area/solution volume ratio was about 0.03 cm⁻¹ and the temperature was controlled to ±1°C. The tests were carried out under both static (open-air) and hydrodynamic (air bubbling) conditions. Some experiments were also conducted under nitrogen purging. Further electrochemical analyses were carried out to investigate the polarization and corrosion potential of the alloys versus time. The polarization curves were recorded potentiodynamically at 0.1666 mVs⁻¹. The temperature was kept at 37°C and controlled to ±1°C by a Vertex thermometer. All curves were recorded under nitrogen. A polarization cell of the type described in ASTM G5 specifications was used with a saturated calomel electrode (SCE) as a reference and two spirals of Pt as counter electrodes.

Specimens for tensile tests were machined from the bars with a gauge length of 40 mm and a diameter of 8 mm. Tests were performed at room temperature with an engineering strain rate of 1,3·10⁻³ s⁻¹.

Hot compression tests were performed to evaluate hot formability of the alloys as a function of temperature and strain rate. Samples of cylindrical geometry and aspect ratio of 2 (diameter 15 mm and length 30 mm) were used for this purpose. Testing was carried out with ram speed ranging from 1 mm/min to 50 mm/min, corresponding to initial strain rates from 5,56·10⁻⁴ s⁻¹ to 2,78·10⁻² s⁻¹. Four testing temperature levels lying in the range 260°C - 450°C were selected for each alloy. However, different values were identified as a function of alloy composition, depending on specific melting point of the alloy (experimentally measured by Differential Scanning Calorimetry (DSC)). The samples were strained in compression down to half of their original height (50% strain) and their flow stress curve was recorded as a function of strain. MoS₂ was used on the bases of the cylindrical specimens as lubricant.

The data on hot compression were used for the application of the Dynamic Material Model, originally proposed by Prasad and co-workers to evaluate material workability as a function of the main process parameters (i.e. temperature, strain, strain rate) [15,16]. According to this approach, the metallurgical phenomena contributing to the power dissipation of the deformation process can be evaluated through a dimensionless parameter, the efficiency of power dissipation (η), which depends on the strain rate sensitivity (m):

$$\eta = \frac{2m}{m+1} \quad m = \frac{\Delta \log \sigma}{\Delta \log \dot{\epsilon}}$$

By mapping the variation of the efficiency parameter as a function of temperature and strain rate, it is possible to draw 3D or contour maps showing the domains of highest efficiency for deformation. It is worth emphasizing that extensive power dissipation is generally achieved by dynamic restoration mechanisms (e.g. recrystallization or recovery) but also through the formation of new surfaces by cavity growth or crack

development. Therefore, microstructural investigations have to be coupled to the model analyses in order to draw fair interpretations of the outputs.

Results and discussions

Representative optical micrographs of the alloys investigated are shown in Figure 1. It can be noticed that in the AZ31 and ZM21 alloys the structure is substantially made up of the Mg-rich solid solution with negligible amounts of other secondary phases. For other alloys, precipitates are observed both at grain boundaries and at the grain interiors. Results of microchemical analyses revealed that in Mg–Al–Zn alloys (AZ series), intermetallic compounds mainly consist of the $Mg_{17}Al_{12}$ phase. In the ZK61 alloy, Zr- and Zn-rich particles were detected whereas in the WE43 alloy, rare earth element accumulated at the grain boundaries.

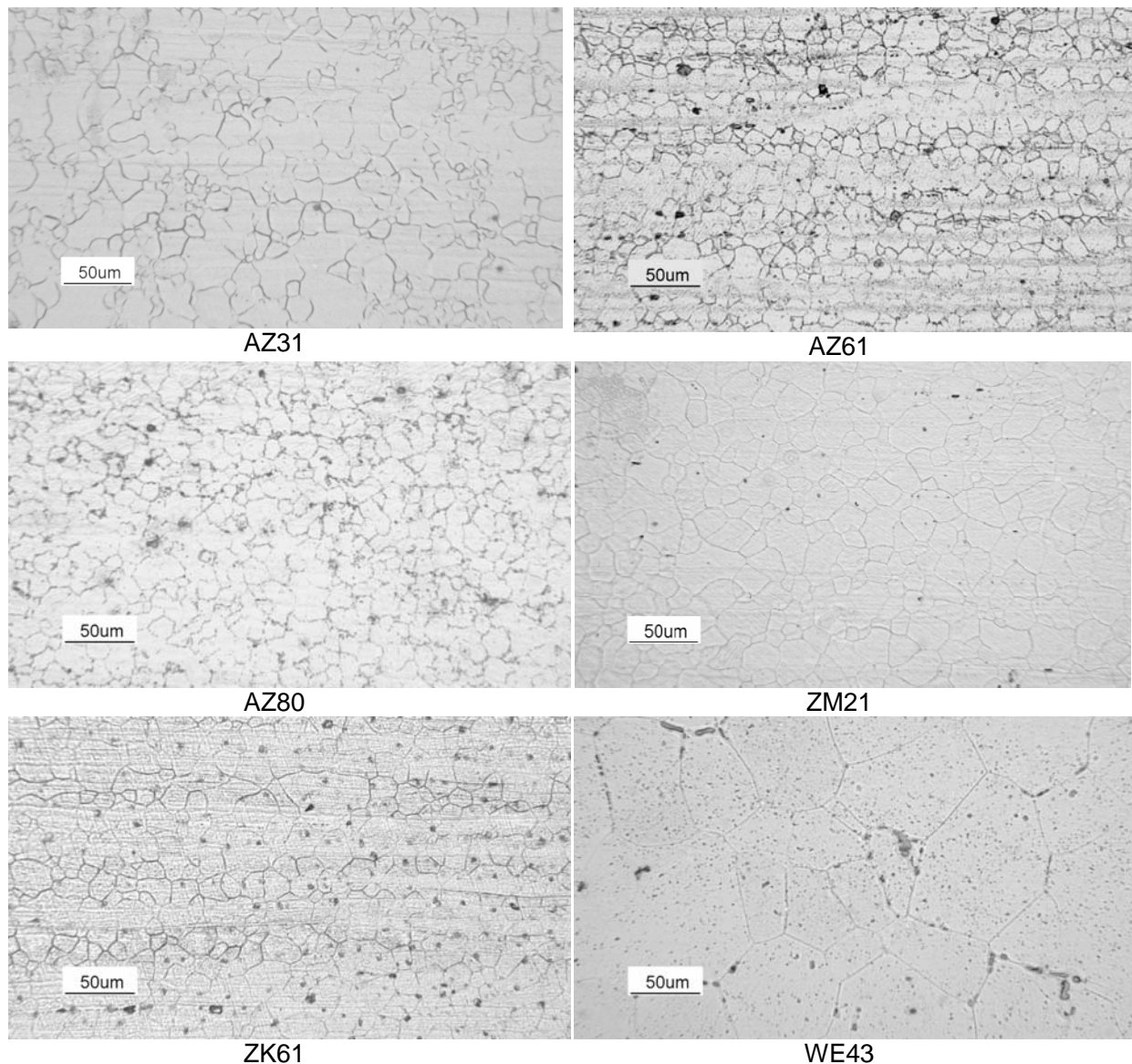


Fig. 1 Representative optical micrographs of the alloys investigated

Table 1 summarizes the corrosion rates of the alloys investigated in SBF solution. The data confirm that, depending on alloying elements, dramatic changes in

corrosion behavior are achieved. An increase in Al content leads to a loss in corrosion resistance whereas addition of rare-earths elements (WE43 alloy) significantly improves the corrosion behaviour of the magnesium alloys.

Figure 2 depicts the potentiodynamic polarization curves recorded under static conditions in SBF solution. Also for this test, the marked effect induced by the presence of Al is evident since all the curves of the AZ series alloys show the presence of a abrupt change of the slope occurring at about the same potential.

Alloy	open-air (mm/year)	air bubbling (mm/year)
ZK61	26,87	24,08
AZ31	10,08	9,36
AZ80	7,92	22,41
ZM21	18,50	14,51
AZ61	9,42	12,28
WE43A	6,82 (N purging)	4,18

Table1. Corrosion rates in SBF solution of the alloys investigated

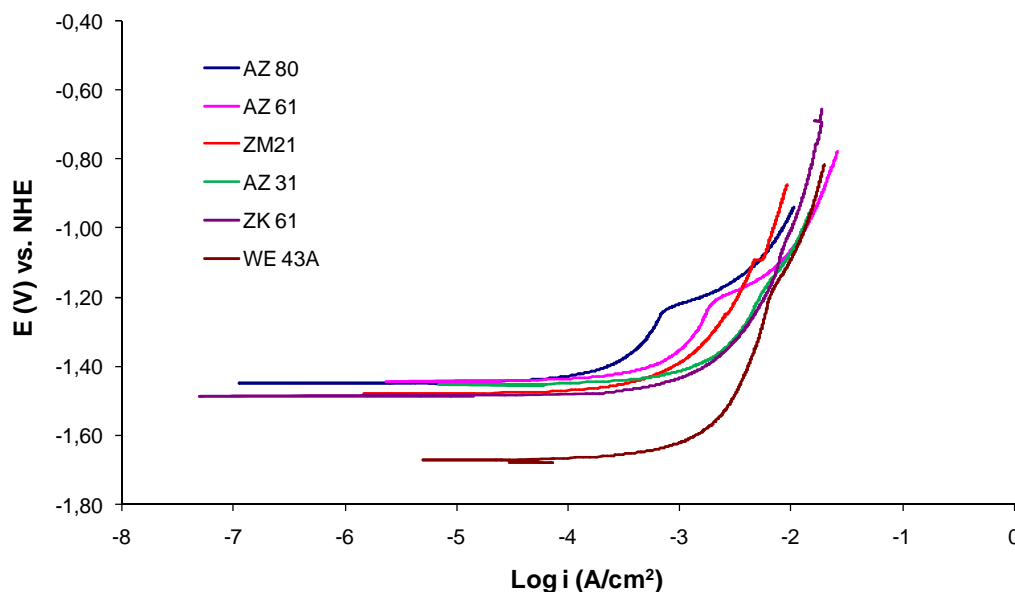


Fig.2 Potentiodynamic polarization curves under static conditions at 37°C in SBF solution

Figure 3 depicts the tensile curves of the materials. The ZM21, AZ31 and AZ61 alloys feature fairly high elongation to fracture values that represent an important pre-requisite for safe stent expansion. As for the strength of the alloys in the as-extruded temper, the AZ80, AZ61 and ZK60 showed the highest ultimate tensile strength, owing to the largest Al content in solid solution.

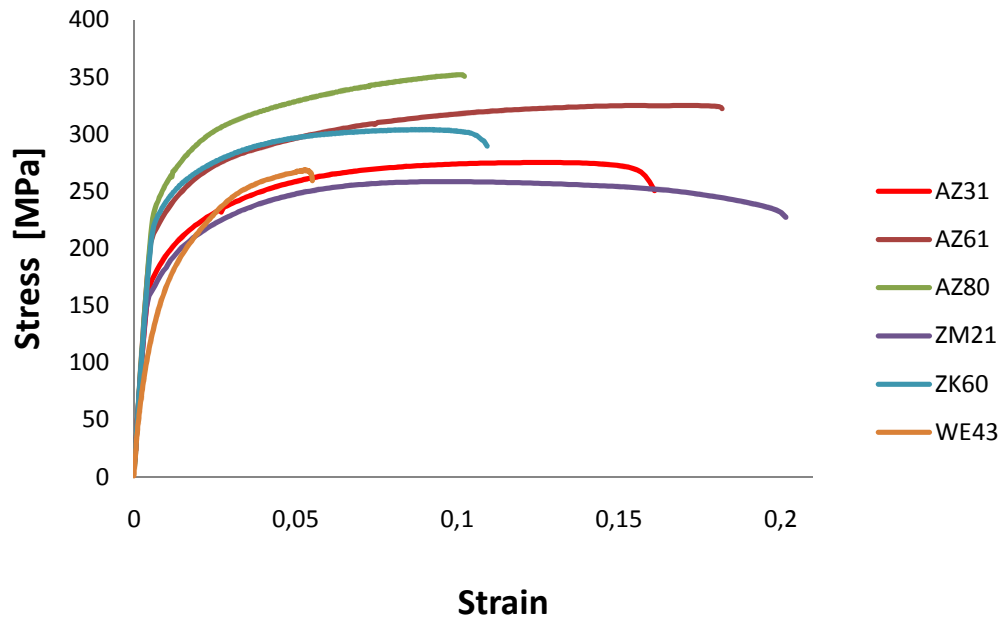


Fig. 3 Stress vs. Strain curves of magnesium alloys

Thermal analyses by DSC were performed with the aim of assessing the precipitation and melting temperatures of the alloys, considering that possible segregation and non-equilibrium constituents could anticipate the appearance of the liquid phase during high-temperature testing. Figure 4 summarizes the curves recorded on heating at a rate of 20°C/min of the alloys investigated. It is confirmed that the ZM21 alloy (with the leaner amount of alloying elements) has the highest values of solidus and liquidus temperatures. As expected, the solidification interval shifts toward lower temperatures and becomes narrower as the concentration of Al in the alloys increases. Based on the above DSC results, the temperature ranges given in table 2 for the hot compression testing were set.

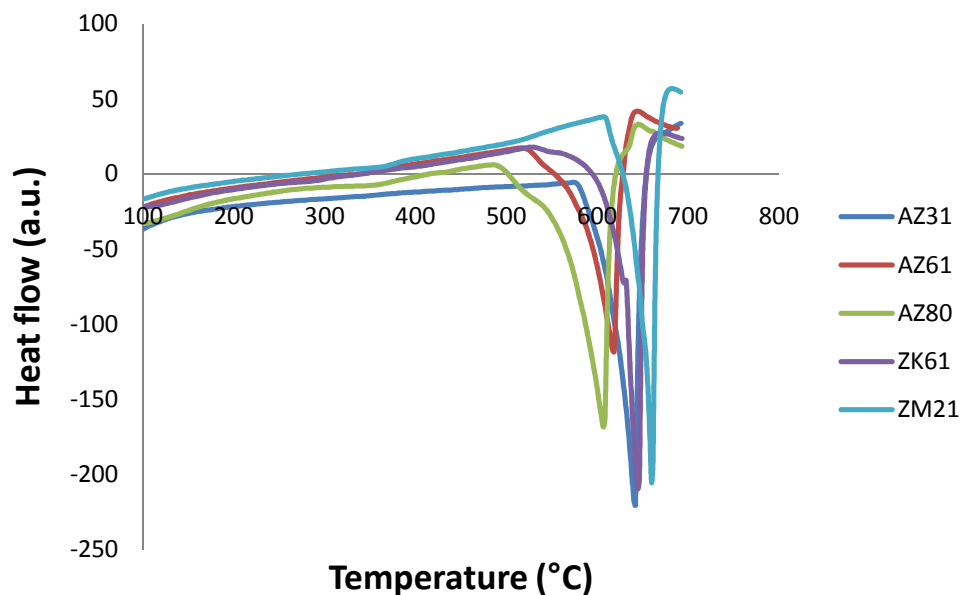


Fig.4 DSC curves of the investigated magnesium alloys recorded during heating at a rate of 20°C/min

Alloy	Temperatures (°C)						
AZ31				350	380	410	450
ZM21				350	380	410	450
ZK61			320	350	380	410	
WE43			320	350	380	410	
AZ61		290	320	350	380		
AZ80	260	290	320	350			

Table 2. Hot compression testing temperatures of the alloys investigated

Typical flow stress vs. strain curves recorded at different temperatures and strain rates are depicted in Figure 5 for the AZ61 alloys. It is shown that the flow stress dramatically increases as the strain rate increases and temperature decreases.

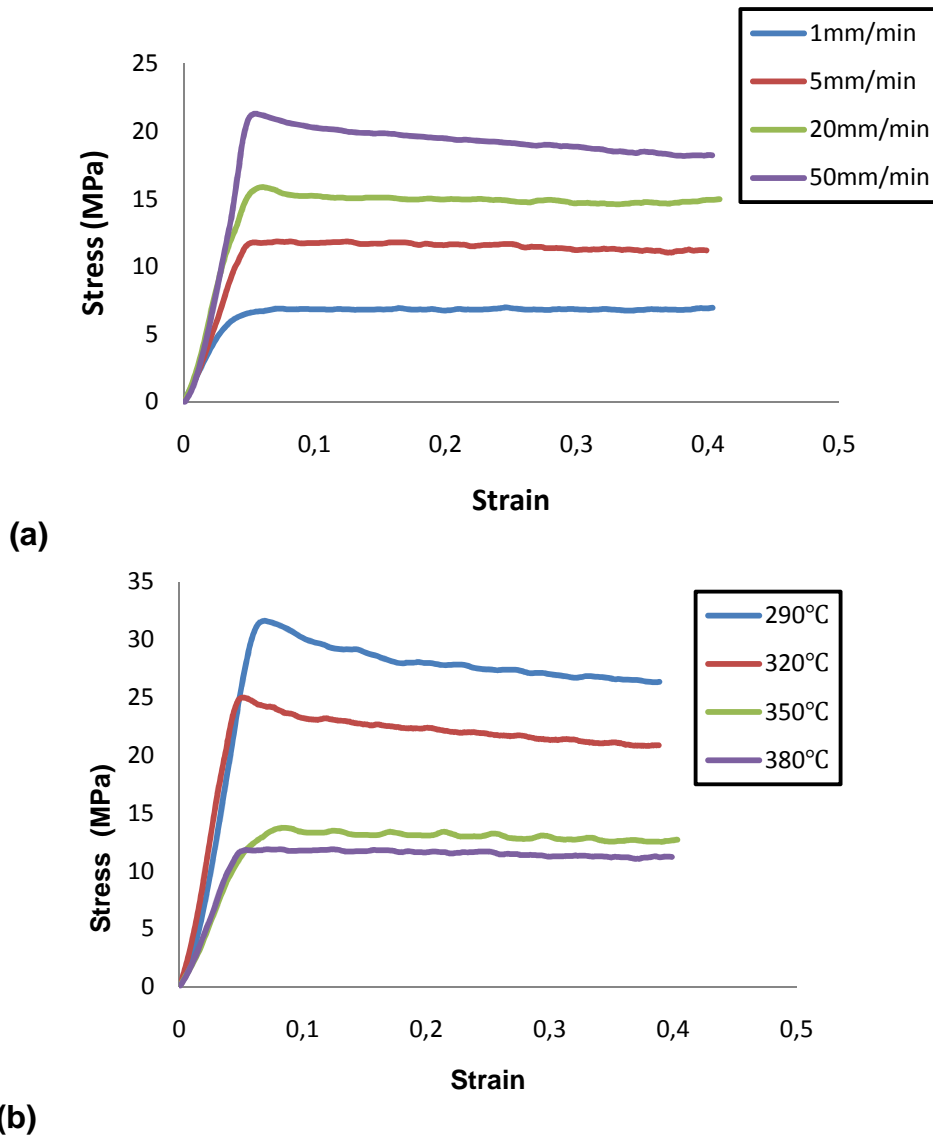


Fig. 5 Representative flow stress curves of the AZ61 alloy tested at 380°C as a function of strain rate (a) and tested at $2,78 \cdot 10^{-3} s^{-1}$ as a function of temperature (b)

By the full set of hot-compression data, the efficiency of power dissipation according to the Dynamic Material Model was calculated and plotted in maps as a function of

temperature and strain rate for each alloy. Figure 6 shows examples of the maps generated for the ZM21 and AZ61 alloys obtained by considering the peak values of the flow stress. From the results given in Figure 6 it can be inferred that for the ZM21 alloy the peak of efficiency, and hence the optimal expected formability conditions, can be found at about 410°C and at slow strain rates. For the AZ61 alloy the optimal hot formability conditions are expected at a slightly lower temperature (about 380°C), still at the lowest strain rate here investigated.

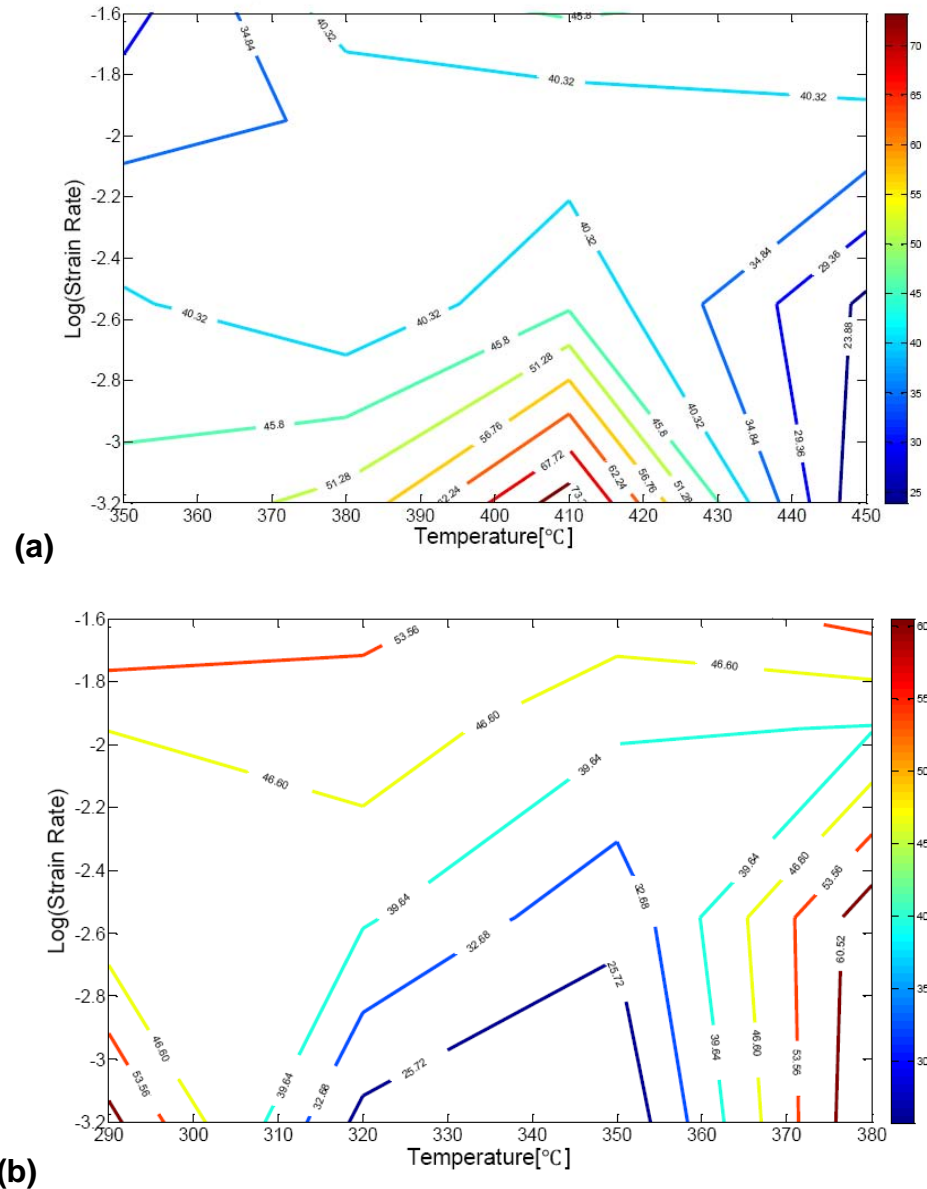
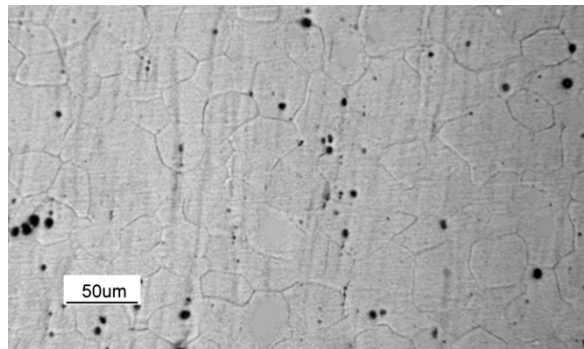
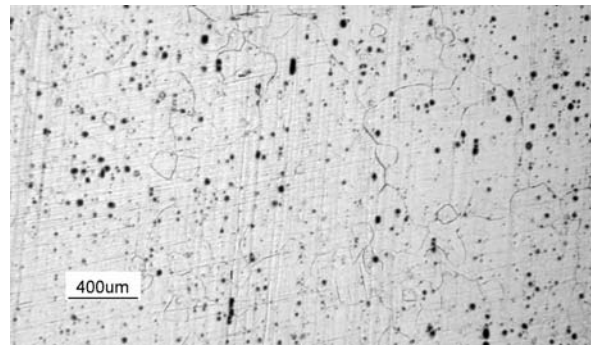


Fig. 6 Efficiency of power dissipation maps of the ZM21 alloy (a) and AZ61 alloy (b)

Finally, analysis of the microstructure resulting after hot compression testing allowed drawing information about possible damage of the alloys as well as about grain size and precipitate evolution, as shown for example in Figure 7 for the ZM21 alloy. As a rule, no cracking or other type of damage was observed in the alloys strained within the investigated temperature and strain rates up to 50%. It was established that the grains kept their original equiaxed shape (suggesting that full recrystallization took place by the end of the test) and their size significantly increased by increasing the temperature and decreasing the strain rate.



380°C, $1,11 \cdot 10^{-2} \text{s}^{-1}$



410°C, $1,11 \cdot 10^{-2} \text{s}^{-1}$

Fig.7 Microstructures after hot deformations of the ZM21 alloy

Conclusions

The experimental study here described was aimed at setting a frame of information and data useful for a full comprehension of the phenomena involved in biodegradable magnesium stent design and manufacturing. The following conclusions can be drawn.

- Corrosion tests either in the form of mass-loss measurements and of potentiodynamic polarization curves performed under static conditions at 37°C in SBF solution showed that, depending on chemical composition, significant modification of the alloy behaviour can be achieved.
- The tensile properties of the six wrought alloys showed that fracture elongation of the order of 17-20% can be achieved in the most ductile materials. Accurate design of the stent shape should be performed in order to limit the room temperature strain imparted to the alloy during stent expansion.
- The hot-formability temperature range of the alloys is soon limited in the upper boundary by reaching the solidus temperature. Hot extrusion for the production of small tubes representing stent precursors should therefore be carried out at reasonably low temperatures to avoid risks of alloy melting.
- Calculation of the efficiency of power dissipation according to the approach suggested by Prasad allowed drawing hot formability maps of the alloys that were used to identify the optimal processing windows.
- Post-deformation microstructural analyses of the samples showed that in proximity to the optimal processing conditions the alloys underwent a recrystallization process and did not show any sign of damage. Their grain size changed depending on actual temperature and strain rate selected.

Acknowledgements

This research was partially supported by a grant from Fondazione Cassa di Risparmio di Trento e Rovereto. L. Petrini, S. Farè and G. Vimercati would also like to acknowledge the financial support of Politecnico di Milano in the frame of the project “Development of bioabsorbable magnesium-alloy innovative stents” dedicated to young researchers (Progetto Giovani Ricercatori 2009).

References

- [1] P. Serruys, P. De Jaegere, F. Kiemeneij, C. Macaya, W. Rutsch, G. Heyndrickx, H. Emanuelsson, J. Marco, V. Legrand, P. Materne, J. Belardi, U. Sigwart, A. Colombo, J. Goy, P. Van De Heuvel, J. Delcan, M. Morel. A comparison of balloon-expandable-stent implantation with balloon angioplasty in patients with coronary artery disease. *N. Engl. J Med.*, 331 (1994) 489-495
- [2] R. Erbel, C. Di Mario, J. Bartunek, J. Bonnier, B. De Bruine, F.R. Eberli, P. Erne, M. Haude, B. Hueblein. Temporary scaffolding of coronary arteries with bioabsorbable magnesium stents: a perspective, non-randomised multicentre trial. *www.lancet.com*, 369 (2007) 1869-1875
- [3] R. Zeng, W. Dietzel, F. Witte, N. Hort, C. Blawert. Progress and challenge for magnesium alloys as biomaterials. *Advanced Biomaterials* (2008) B3-B14
- [4] A. Colombo, E. Karvouni. Biodegradable stents: "fulfilling the mission and stepping away". *Circulation* 102, (2000) 371-373
- [5] H. Muller. Development of metallic bioabsorbable intravascular implants. In: N. Chakf and B. Durand (eds.), 'ESVB 2009 New Technologies in Vascular Biomaterials. Connecting Biomaterials to Arterial Structures', Chapter 3, Europrot, Strasbourg, France (2009), 23-32
- [6] M. Maeng, J.O. Jensen, E. Falk, H.R. Andersen, L. Thuesen. Negative vascular remodeling after implantation of bioadsorbable magnesium alloy stents in porcine coronary arteries: a randomized comparison with bare-metal and sirolimus-eluting stents. *Heart* 95 (2009) 241-246
- [7] J.A. Ormiston, P.W.S. Serruys. Bioabsorbable coronary stents. *Circ Cardiovasc Interv* 2 (2009) 255-260
- [8] J.E. Gray, B. Luan. Protective coatings on magnesium and its alloys – a critical review. *J. Alloys and Comp.*, 336 (2002) 88-113
- [9] W. Wu, L. Petrini, D. Gastaldi, M. Vedani, F. Migliavacca. Finite element shape optimization for biodegradable magnesium alloy stents. *Ann. Biomed. Eng.*, submitted for publication (2010)
- [10] D. Gastaldi, V. Sassi, L. Petrini, M. Vedani, S. Trasatti, F. Migliavacca. Continuum damage model for bioresorbable magnesium alloy devices. Application to endovascular coronary stents. *J. Mech. Behavior of Biomed. Mat.*, submitted for publication (2010)
- [11] Y. Uematsu, K. Tokaji, M. Kamakura, K. Uchida, H. Shibata, N. Bekku. Effect of extrusion conditions on grain refinement and fatigue behavior in magnesium alloys. *Mater. Sci. Eng.*, A434 (2006) 131-140
- [12] T. Murai, S. Matsuoka, S. Miyamoto, Y. Oki. Effects of extrusion conditions on microstructure and mechanical properties of AZ31 magnesium alloy extrusions. *J. Mater. Proc. Technol.*, 141 (2003) 207-212
- [13] J. Swiostek, J. Goken, D. Letzig, K.U.Kainer. Hydrostatic extrusion of commercial magnesium alloys at 100°C and its influence on grain refinement and mechanical properties. *Mater. Sci. Eng.*, A424 (2006) 223-229
- [14] M. Chandrasekaran, Y.M. Shyan John. Effect of materials and temperature on the forward extrusion of magnesium alloys. *Mater. Sci. Eng.*, A381 (2004) 308-319
- [15] Y.V.R.K. Prasad, T. Seshacharyulu. Modelling of hot deformation for microstructural control. *International Materials Reviews*, 43, 6 (1998) 243-258
- [16] O. Sivakesavam, I.S. Rao, Y.V.R.K. Prasad. Processing maps for hot working of as cast magnesium. *Mater. Sci. Techn.*, 9 (1993) 805-810